



Research article

Photophysical properties of ammonium, pyrrolidinium, piperidinium, imidazolium, and pyridinium as a guide to prepare ionic-organic hybrid materials



Yuly Kusumawati ^{a,*}, Athar L. Ivansyah ^{b,c}, Badrut T.I. Ali ^a, Kiki A. Kurnia ^d, Aulia S. Hutama ^e, Hamzah Fansuri ^a

^a Department of Chemistry, Faculty of Science and Data Analytics, Institut Teknologi Sepuluh Nopember, ITS Campus Sukolilo, East Java, Surabaya, 60111, Indonesia

^b Master Program in Computational Science, Faculty of Mathematics and Natural Sciences, Institut Teknologi Bandung, Jl. Ganesh No. 10, West Java, Bandung, 40132, Indonesia

^c Analytical Chemistry Division, Department of Chemistry, Faculty of Mathematics and Natural Sciences, Institut Teknologi Bandung, Jl. Ganesh No. 10, West Java, Bandung, 40132, Indonesia

^d Department of Chemical Engineering, Faculty of Industrial Technology, Institut Teknologi Bandung, Jalan Ganesh No 10, West Java, Bandung, 40132, Indonesia

^e Department of Chemistry, Faculty of Mathematics and Natural Science, Universitas Gadjah Mada, Sekip Utara, Bulaksumur, Sleman, 55281, Indonesia

ARTICLE INFO

Keywords:

Ionic liquid

Fluorescence

Phosphorescence

TDDFT

DFT

ABSTRACT

Ionic liquid cations (ILCs) have been utilized in hybrid organic-inorganic perovskites (HOIPs) to enhance their photoluminescence performance. However, the high number of possible cations and anions needed to form ILCs makes the experimental measurement time and cost consuming. Computational methods that could assist the selection of ILCs for this task-specific application are highly desirable. Therefore, in this work, the photophysical properties of various ILCs, including linear aliphatic, five-membered, and six-membered cyclic aliphatic, and aromatic ILCs, were investigated using density functional theory (DFT) and time-dependent density functional theory (TDDFT). Fluorescence and phosphorescence were analyzed using excited state dynamics (ESD) modules on ORCA at the B3LYP/def2TZVP level theory. All the investigated cations show fluorescence spectra either the UV or visible range. The cations with long-chain branches show fluorescence spectra in the visible range. Five membered rings show the phosphorescence spectra in the visible range, while the six-membered rings show the phosphorescence spectra in the near-infrared range.

1. Introduction

Photoluminescence is an emission process of light that follows a photon absorption process. There are two kinds of photoluminescence, fluorescence and phosphorescence. Phosphorescence requires an inter-system crossing process before emission occurs. Through this process, the singlet states of excited electrons change to triplet states. This phosphorescence process takes much more time compared than fluorescence [1]. The application of photoluminescence covers many fields, including device displays [2, 3], imaging [4, 5] biomarkers [6], information storage [7], and sensor detectors [8]. Various potential materials have been developed for these purposes, including all-inorganic compounds [4, 5, 8], all-organic compounds [9, 10], and organic-inorganic hybrid materials [2, 4, 6, 9]. In contrast to all-inorganic materials that require high temperature for synthesis through the solid-state method,

organic-inorganic hybrid materials can be synthesized via simpler methods such as solvothermal [12, 13, 14], hydrothermal [15, 16], or diffusion methods [17, 18]. Moreover, hybrid materials will have the properties of their components simultaneously, either inorganic or organic [11, 18, 19]. In the last five years, incorporating ionic liquid cations (ILCs) into organic-inorganic hybrid perovskite materials has shown the potential to increase the photoluminescent properties [19].

ILCs are the salts that exist in the liquid phase at a temperature below 100 °C. There are many reports of incorporating ionic liquid cations (ILCs) into photoluminescent hybrid materials. ILCs couple either with halometal [18, 19, 20] or hybrid organic inorganic perovskites (HOIPs) [12, 21, 22]. The presence of ILCs influences the packing density in the structure. The more compact structure will have a less nonradiative transition and, consequently, a higher quantum yield [19]. Thus, the ILCs structure will become an important consideration for applications as

* Corresponding author.

E-mail address: y_kusumawati@chem.its.ac.id (Y. Kusumawati).

mentioned earlier. For example, *Jin et al.* have shown that using ILCs with a longer alkyl chain length will result in a lower packing density and decrease the phosphorescence quantum yield [22]. The presence of ionic liquids can also induce the photoluminescence switching phenomenon. This phenomenon appears because of the phase transition provoked by the rotational isomer of the ILCs. For example, the different conformations of 1-butyl-2,3-dimethyl imidazolium (BMMIM) in the (2)-[BMMIM] $[\text{BiCl}_4(2,2'\text{-bpy})]$ ($2,2'\text{-bpy}$ = 2,2'-bipyridyl) crystal polymorph give photoluminescence switching from a cyan crystal to a greenish crystal [12]. The photoluminescence ILCs of the hybrid material also contribute to the photoluminescence spectrum, resulting in dual-band emission. For example, $\pi \rightarrow \pi^*$ propylammonium emission spectra of perovskite [1, 5-bis(1-methylimidazolium)pentane]- $[\text{PbBr}_3]_2$ [23]. The investigation of ILC structure-photophysical property relationships is important in designing or choosing molecules that fulfil the desired properties. *Chen et al.* pointed out the following criteria should be addressed to obtain a high quantum yield photoluminescence of ILCs, (1) Have a little structural change during the electronic transition process; (2) The frontier orbitals (HOMO = The Highest Occupied Molecular Orbital and LUMO = The Lowest Unoccupied Molecular Orbital) located in the same entire location and the positive-charge is centered; (3) having the electron-rich system [9].

In this work, we investigate the mapping of ILC structure-photophysical property relationships through a computational study. Nine ILCs were observed in this study ethylammonium, propylammonium, pyrrolidinium, piperidinium, imidazolium, 1-ethyl-3-methylimidazolium (EMIM), 1- butyl-3-methylimidazolium (BMIM), pyridinium, and phenylbutylammonium (PBA), are representative of linear structures, cyclic five- and six-membered-rings and aromatic five- and six-membered-rings [Figure 1]. In addition, some of these ILCs have been used in the HOIP perovskites such as EMIM [22], BMIM [24, 25], piperidinium, pyridinium [20] and PBA [11]. The investigated properties included (1) the optical properties; UV-Vis absorption, fluorescence, and phosphorescence spectra; and (2) the electronic properties; frontier molecular orbital visualization and charge distribution.

2. Computational methods

All calculations in this research were performed by using the ORCA 4.2.0 software package [26]. The Becke, 3-parameter, Lee-Yang-Parr

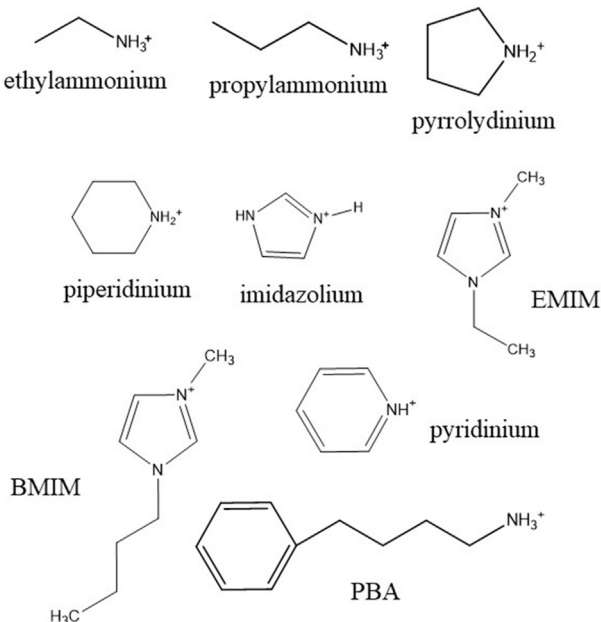


Figure 1. The observed ILCs in this research.

(B3LYP) hybrid functional [27, 28] coupled with the basis set polarized triple-zeta valence (TZV) quality plus polarization function (def2-TZVP) [29] was chosen for the calculation. The geometry optimization of the ground state followed by the vibration analysis of the optimized geometry was carried out by density functional theory (DFT). The optimization geometry was conducted without any constraint on the bond, angle, or symmetry. The electron excitation energy and the optimization of the excitation state geometry (including singlet and triplet states) were carried out using time-dependent density functional theory (TDDFT). Fluorescence and phosphorescence spectrum analyses were conducted by using the Excited State Dynamics (ESD) module of ORCA 4.2.0 [30]. Many studies have been performed using this module, and the results show satisfactory data [31, 32, 33]. Visualization of the results including frontier molecular orbital analysis was performed using Chemcraft molecular visualization programs [34]. All the calculations to investigate the photoluminescence study were performed in the gas phase. However, the calculation that considered the solvation effect for the ground state was performed using the CPCM continuum model using acetonitrile as a solvent [35]. Acetonitrile was chosen as a solvent because the literature shows experimental results using this solvent [36].

3. Results and discussion

3.1. Ground state-, singlet excitation state- and triplet excitation state optimized geometry

The optimized geometry of all observed molecules in their ground states, singlet excitation states, and triplet excitation states are presented in Tables S1–S9 (Supplementary Material). The singlet excited states and the ground state structures of acyclic ethylammonium and propylammonium show the largest difference among the others. Table S1 shows that the bond lengths of N11 and H9 increase from 1.023 Å in the ground state to 1.897 Å in the singlet excited state. This phenomenon is also observed for the cyclic aliphatic molecules, piperidinium, and pyrrolidinium. Both structures have the optimized geometry in a planar structure in the ground states, as shown in Table S3–S4. The optimized structure in singlet excited states shows that they are no longer in a planar structure but in a chair conformation. As observed in the acyclic molecules, the hydrogen atom attached to the nitrogen atom tends to be far away in the excited states.

The difference in unoccupied molecular orbital (MO) energy in the ground states and the singlet excitation states confirms the different structures in these states. The calculated occupied MO As shown in Table 1 aliphatic ions, either linear or cyclic such as ethylammonium, propylammonium, piperidinium, and pyrrolidinium have different unoccupied molecular orbital (MO) energies in the ground states and excitation states in the range of 4.25–5.23 eV. This means that much energy is allocated for the nonradiative process. This phenomenon will result in a low quantum yield for the photoluminescence process [37].

The presence of conjugated- π bonding in aromatic ILCs makes them have a rigid structure. Table 1 shows that all aromatic ILCs have ground-state-excited-state energy levels and singlet-excited-state-energy-level differences that are smaller than those of aliphatic ILCs. These results indicate that more energy is needed for stabilizing the excited singlet state species.

Tables S1–S10 also present the optimized structure of the triplet excited states. The optimized triplet excitation state structures show different structures with singlet excited states. These results confirm that there is a change after intersystem crossing. The triplet excited states of acyclic aliphatic and cyclic aliphatic structures have many changes compared to their ground state structures. The hydrogen atom attached to the nitrogen atom in ethyl ammonium, piperidinium, and pyrrolidinium is broken apart. However, triplet excited states and singlet excited states of aromatic molecules almost no change. The presence of an alkyl chain in the substituent provides a possibility for structural change. This

Table 1. The energy level of the occupied and unoccupied molecular orbital involved in the electronic transition.

ILCs	Ground state		Singlet excited state	The ground states and singlet excited state unoccupied MO difference (eV)
	Occupied MO (eV)	Unoccupied MO (eV)	Unoccupied MO (eV)	
Ethylammonium (H-1→ L)	-15.4679	-5.3512	-10.5799	5.2287
Propylammonium (H-2→ L)	-14.5043	-5.2502	-10.3355	5.0853
Pyrrolidinium (H-1→ L)	-14.6831	-4.9343	-9.3597	4.4254
Piperidinium (H-2→ L)	-13.6795	-4.9286	-9.1796	4.2510
Imidazole (H→ L)	-12.5894	-5.8908	-6.3920	0.5012
EMIM (H→ L+1)	-11.7957	-4.2311	-4.4439	0.2128
BMIM (H → L+1)	-11.6912	-4.1179	-4.3516	0.2337
Pyridinium (H→ L)	-13.0931	-7.1324	-7.3093	0.1769
PBA (H→ L+1)	-8.9605	-3.39247	-3.9351	0.542599

process requires energy and causes the phosphorescence efficiency to decrease [26].

3.2. Analysis of frontier molecular orbital and charge distribution

The calculated frontier orbital of the observed molecules is displayed in [Figure 2](#). The MOs involved in the electronic transitions are not always from HOMO and LUMO. [Table 1](#) displays the frontier MOs involved in the electronic transition for each of the ILCs, some of which occurred from H-1 or to L+1 to simplify we mention here as HOMO and LUMO. All ammonium-aliphatic molecules have a HOMO area in the C–C bond, whereas the LUMO is located in the nitrogen region. All the frontier orbital molecules of aromatic compounds are well delocalized in the ring. [Chen et al.](#) have shown that to obtain a high quantum yield in photoluminescence the HOMO and LUMO should be delocalized as well as the positive charge [9]. The charge distribution in molecules is shown in Figures 3, 4, and 5. All five-membered aromatic compounds (BMIM, EMIM, and imidazolium) show a well-centered positive charge on the carbon atom that is located between the nitrogens. The cyclic aliphatic PBA also has a centered positive charge due to the presence of ammonia

at the substituent edge. However, because the substituent chain length is long (four carbon atoms), the LUMO position is separated from the HOMO. Thus, attaching the ring with a short ammonia substituent will direct positive charge delocalization.

3.3. The absorption, fluorescence, and phosphorescence spectra

The calculated absorption spectra of the observed molecules in the gas phase and solvation effect are presented in [Figure 6](#). All the observed molecules absorb photons in the UV-C range except PBA, which absorbs the photons in the UV-A range. Based on the literature [36], protonated pyridine (pyridinium) has a UV absorption peak at 256 nm. The calculation used the same method but with the solvation condition in acetonitrile, giving the absorption peak at 222 nm ([Figure 6](#)), which only differs by approximately 5 nm compared to the result in the gas phase. Overall, the calculation difference with the experiment for pyridinium is approximately 15.2% compared to the gas phase and 13.2% compared with the same solution.

The calculated fluorescence spectra show that all molecules show fluorescence spectra in either UV or visible light (Figures S1 – S9 in

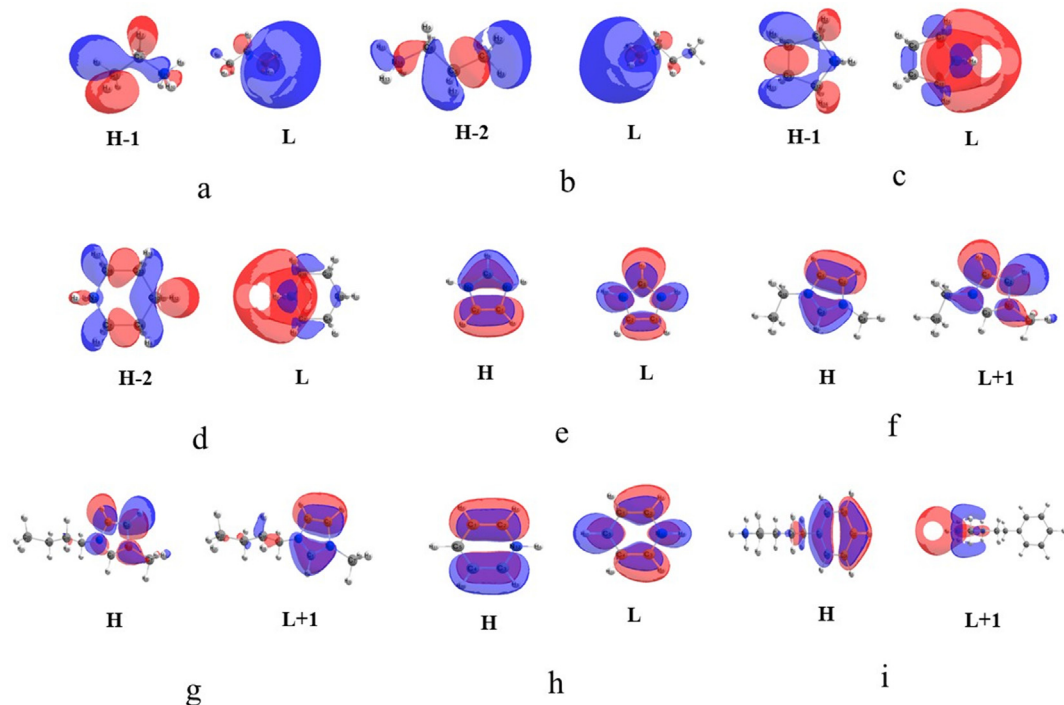


Figure 2. The profile of frontier molecular orbitals involved in the electronic transition of (a) ethylammonium (b) propylammonium (c) pyrrolidinium (d) piperidinium (e) imidazolium (f) EMIM (g) BMIM (h) pyridinium and (i) PBA.

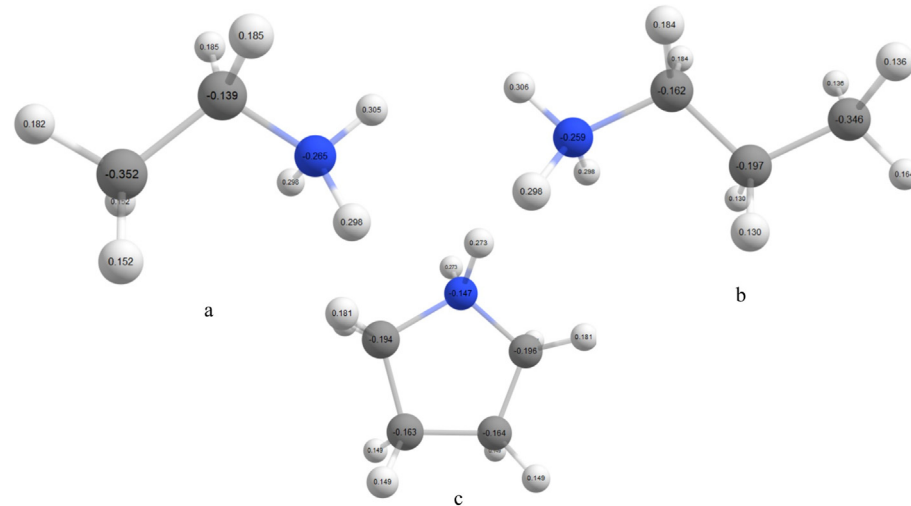


Figure 3. The calculated Mulliken charge of (a) ethylammonium (b) propylammonium and (c) pyrrolidinium.

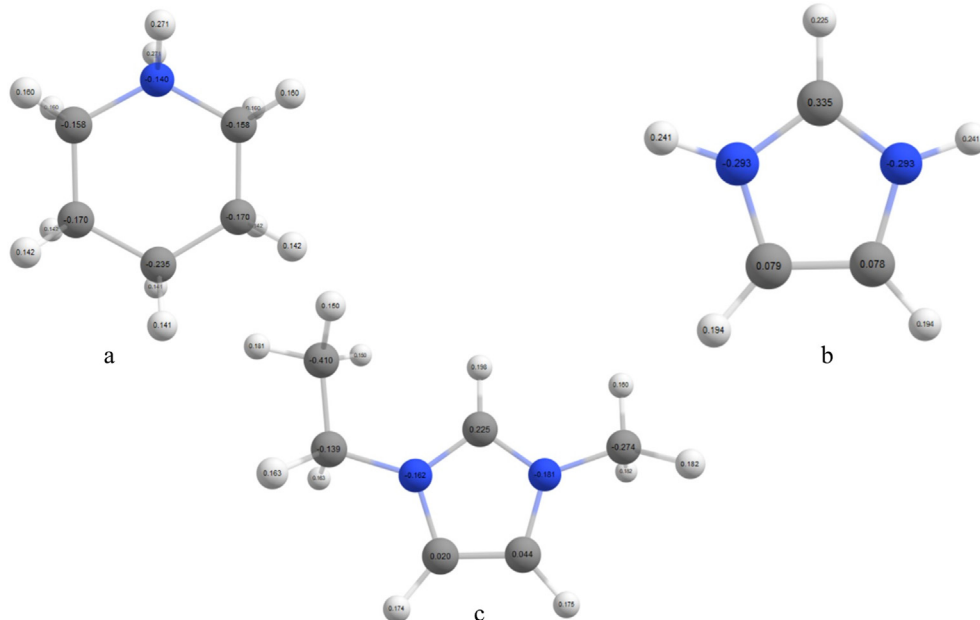


Figure 4. The calculated Mulliken charge of (a) piperidinium (b) imidazolium and (c) EMIM.

Supplementary Material). The following molecules show fluorescence spectra in the visible range: BMIM, piperidinium, and PBA. The remaining molecules show fluorescence spectra in the UV range, either UV-A, UV-B, or UV-C.

The calculated phosphorescence spectra show that only EMIM, pyrrolidinium, and imidazolium show phosphorescence spectra in the visible range. Piperidinium and pyridinium have phosphorescence spectra in the near-infrared range. This result shows that all five-membered ring compounds show phosphorescence spectra in the visible region, except BMIM, which does not show phosphorescence spectra. The long-chain substituent in the ring seems to hinder the intersystem crossing process. This is also observed in the PBA and molecules with linear structures (ethylammonium, propylammonium, and PBA).

The ability for intersystem crossing in ILC molecules is also promising for phosphorescence if they combine with metal halides to form HOIPs. Table 2 shows summary of the calculated fluorescence and phosphorescence ILC molecules that have been used in HOIPs. The photoluminescence properties of $[BMIM]_2SBCl_5$ are initiated by BMIM through the intra ligand charge transfer (ILCT) process [24]. On the other hand,

the existence of another organic species in the anion will make a difference in photoluminescence. Shen et al. confirmed that $[BMIM][BiCl_4(2',2'-bpy)]$ ($2',2'$ -bpy = $2,2'$ -bipyridine) shows a phosphorescence spectrum at 524–530 nm. The ligand $2,2'$ -bpy is more responsible for the phosphorescence properties [25]. Jin et al. also showed through DFT study that $2,2'$ -bipyridyl-1,10-dioxide (bp2do) is responsible for the photoluminescence property of $[EMIM]BiCl_4(bp2do)$, EMIM = 1-ethyl-3-methylimidazolium [22]. However, ILCs have a role in compound packing that finally increases the quantum yield [22, 34].

The fluorescence and phosphorescence rate constants of the molecules were extracted from the calculation and are presented in Table 3. The fluorescence and phosphorescence lifetimes were then calculated using Eq. (1). Both calculated lifetimes only indicate the radiative lifetime and do not include the non-radiative lifetime.

$$\tau_{av} = \frac{1}{k_{av}} \quad (1)$$

where τ_{av} is the average radiative lifetime (s) and k_{av} (s^{-1}) is the average fluorescence of the phosphorescence rate constant.

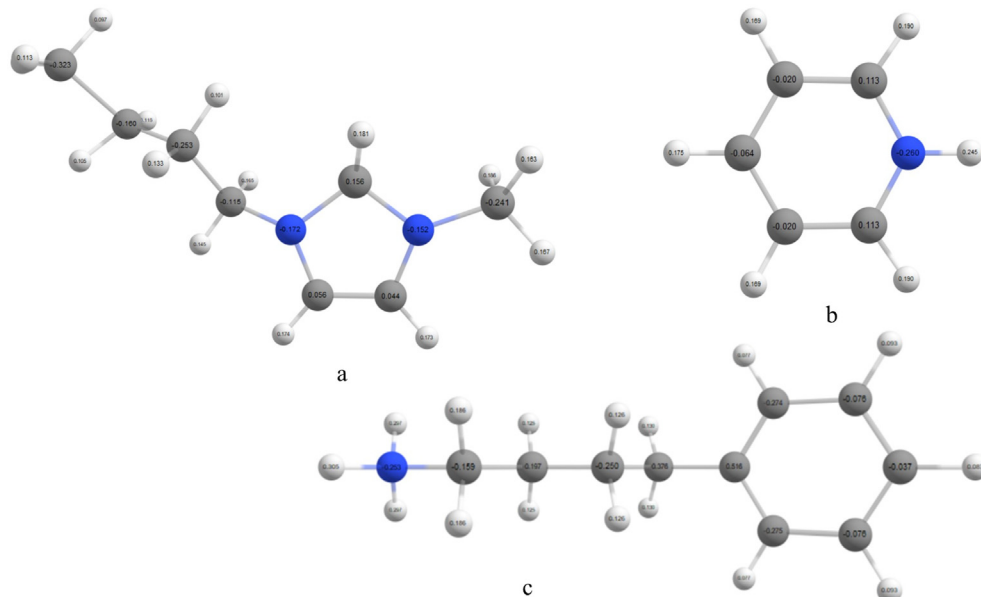


Figure 5. The calculated Mulliken charge of (a) BMIM (b) pyridinium and (c) PBA.

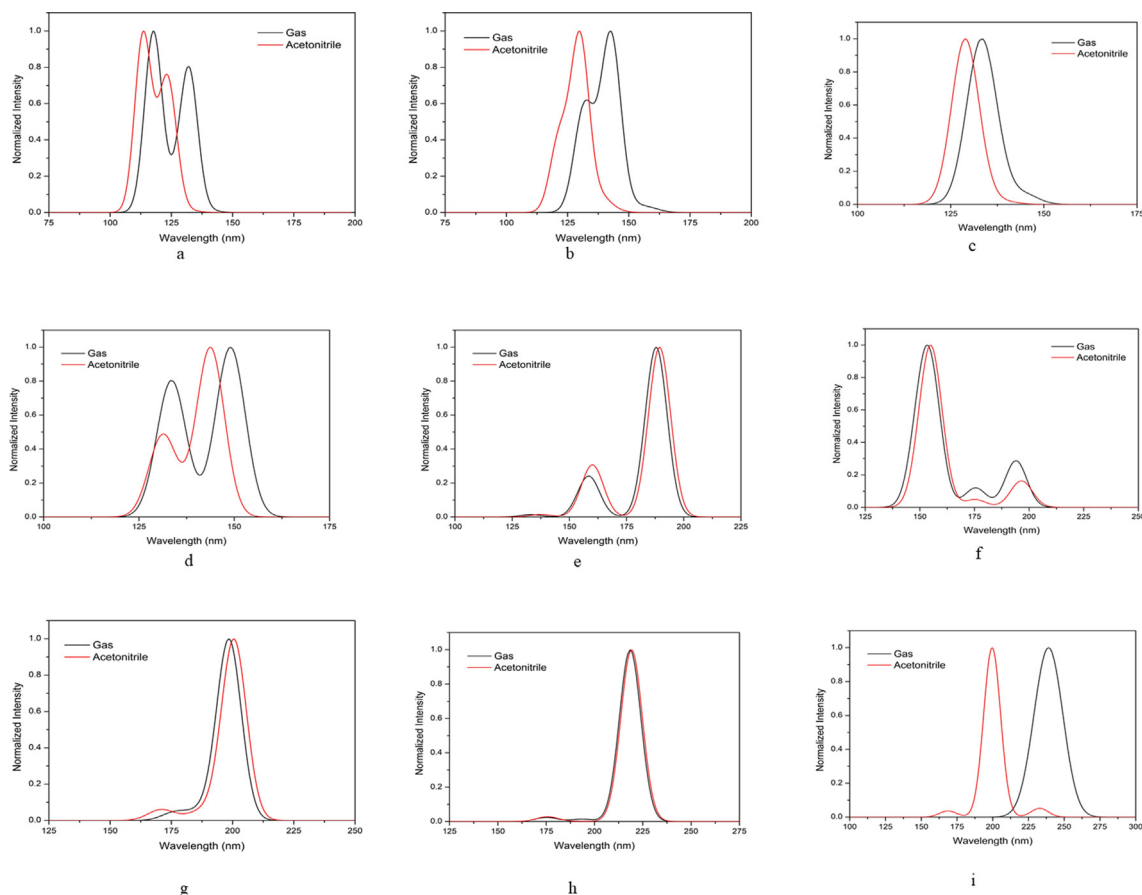


Figure 6. UV-Vis absorption spectra in the gas phase and acetonitrile of (a) ethylammonium (b) propylammonium (c) pyrrolidinium (d) piperidinium (e) imidazolium (f) EMIM (g) BMIM (h) pyridinium and (i) PBA.

Table 3 shows that the fluorescence lifetimes are shorter than the phosphorescence lifetimes as expected. Propylammonium has a longer radiative fluorescence and phosphorescence lifetime than the ethylammonium. Thus, an increase in the alkyl chain number increases the radiative lifetime. Aromatic six-membered ring ILCs have longer radiative

fluorescence and phosphorescence lifetimes than the five-membered ring ILCs. The cyclic aliphatics give different radiative lifetimes. The fluorescence radiative lifetime of piperidinium is longer than that of pyrrolidinium, while the phosphorescence lifetime is shorter. The shorter the lifetime is, the higher the quantum yield obtained. The nonradiative

Table 2. The calculated fluorescence and phosphorescence ILCs and the other HOIPs related to the ILCs and their photoluminescence properties.

ILCs	Result in this study (nm)			Experiment/Computational study (nm)	Photoluminescence properties	Ref.
	λ_{abs} (nm)	λ_{fluor} (nm)	λ_{phos} (nm)			
EMIM	159.7	223.7	755.5	[EMIM]BiCl ₄ (bp2do) bp2do = 2,2'-bipyridyl-1,10-dioxide	Phosphorescence at 450 nm	[22]
BMIM	172.5	465.4	-	[BMIM] ₂ SbCl ₅	Fluorescence at 460 nm	[24]
				[BMIM][BiCl ₄ (2,2'-bpy)] (2,2'-bpy = 2,2'-bipyridine)	Phosphorescence at 524–530 nm	[25]
Piperidinium	365.6	486.7	911.2	PipPbBr ₃ (Pip = Piperidinium)	Fluorescence at 630 nm (77K)	[20]
Pyridinium	217	238.4	947.3	PyPbBr ₃ (Py = pyridinium)	Fluorescence at 650 nm (77K)	
PBA	240.3	474.4	-	PBABr ₂ (Cs _{0.7} FA _{0.3} PbBr ₃) Cs _{0.7} FA _{0.3} PbBr ₃	Fluorescence at 439 nm and 462 nm (room temperature)	[11]

Table 3. The calculated fluorescence rate constant, fluorescence radiative lifetime, phosphorescence rate constant and phosphorescence radiative lifetime.

ILC	Fluorescence rate constant (s ⁻¹)	Fluorescence radiative lifetime (s)	Phosphorescence rate constant (s ⁻¹)			Average phosphorescence rate constant (s ⁻¹)	Phosphorescence radiative lifetime (s)
			1	2	3		
Ethylammonium	1.58 x 10 ⁷	6.33 x 10 ⁻⁸	2.53 x 10 ⁻²	3.77 x 10 ¹	8.61 x 10 ¹	4.13 x 10 ¹	2.42 x 10 ⁻²
Propilaminium	6.02 x 10 ⁶	1.66 x 10 ⁻⁷	2.71 x 10 ⁻⁴	3.83 x 10 ⁻²	4.94 x 10 ⁻²	2.93 x 10 ⁻²	3.41 x 10 ¹
BMIM	3.23 x 10 ⁷	3.10 x 10 ⁻⁸	1.17 x 10 ⁻²	4.53 x 10 ⁻²	1.47 x 10 ⁻³	1.95 x 10 ⁻²	5.14 x 10 ¹
EMIM	1.43 x 10 ⁸	7.01 x 10 ⁻⁹	3.99 x 10 ⁻³	5.08 x 10 ⁻¹	1.36 x 10 ⁻¹	2.16 x 10 ⁻¹	4.63
Piperidinium	6.72 x 10 ⁵	1.49 x 10 ⁻⁶	5.84 x 10 ⁻³	4.25 x 10 ³	4.29 x 10 ³	2.85 x 10 ³	3.51 x 10 ⁻⁴
Pyrrolidinium	5.61 x 10 ⁶	1.78 x 10 ⁻⁷	1.26 x 10 ⁻¹	2.36 x 10 ¹	2.46 x 10 ¹	1.61 x 10 ¹	6.20 x 10 ⁻²
Pyridinium	8.47 x 10 ⁷	1.18 x 10 ⁻⁸	6.15 x 10 ⁻³	1.85 x 10 ⁻⁴	1.39 x 10 ⁻³	2.57 x 10 ⁻³	3.89 x 10 ²
PBA	2.02 x 10 ⁶	4.95E x 10 ⁻⁷	5.34 x 10 ⁻⁴	2.32 x 10 ⁻⁴	1.70 x 10 ⁻⁴	3.12 x 10 ⁻⁴	3.20 x 10 ³
Imidazolium	2.38 x 10 ⁸	4.19 x 10 ⁻⁹	1.53 x 10 ⁻²	1.01 x 10 ⁻³	6.20 x 10 ⁻²	2.61 x 10 ⁻²	3.83 x 10 ¹

process due to the flexibility of molecules and the environment must be considered as it will decrease the quantum yield. For rigid environments such as solid crystals, the radiative lifetime will determine the quantum yield due to the restriction of the nonradiative process [38, 39].

4. Conclusions

The investigation of the photoluminescence properties in relation to the structure and electronic properties was performed. The longer alkyl chain in the substituent provoked more energy needed for structure stabilization in the excitation state except for PBA which has an ammonium moiety at the substituent edge. The five-membered rings show phosphorescence spectra in the visible range while the six-membered rings show phosphorescence spectra in the near-infrared region. The radiative lifetime of aromatic five-membered rings is shorter than the radiative lifetime of six-membered rings. The study of the five-membered ring endowed with a short ammonium moiety will be of interest. The study also needs to be expanded by considering the anion interaction to consider the effect of a flexible environment.

Declarations

Author contribution statement

Yuly Kusumawati: Conceived and designed the experiments; Analyzed and interpreted the data; Wrote the paper.

Athar L. Ivansyah: Performed the experiments; Analyzed and interpreted the data.

Badrut T. I. Ali: Performed the experiments.

Kiki A. Kurnia, Aulia S. Hutama: Analyzed and interpreted the data.

Hamzah Fansuri: Contributed reagents, materials, analysis tools or data.

Funding statement

This work was supported by Directorate General of Higher Education, Ministry of Education and Culture, Republic of Indonesia (1044/PKS/ITS/2021).

Data availability statement

Data included in article/supplementary material/referenced in article.

Declaration of interests statement

The authors declare no conflict of interest.

Additional information

Supplementary content related to this article has been published online at <https://doi.org/10.1016/j.heliyon.2022.e09121>.

References

- Valeur, B., M.N. Berberan-Santos, A brief history of fluorescence and phosphorescence before the emergence of quantum theory, *J. Chem. Educ.* 88 (6) (Jun. 2011) 731–738.
- G. Pathak, G. Hegde, V. Prasad, Octadecylamine-capped CdSe/ZnS quantum dot dispersed cholesteric liquid crystal for potential display application: investigation on photoluminescence and UV absorbance, *Liq. Cryst.* 48 (4) (Mar. 2021) 579–587.
- Y. Ge, L. Meng, Z. Bai, H. Zhong, Linearly polarized photoluminescence from anisotropic perovskite nanostructures: emerging materials for display technology, *J. Infect. Dis.* 20 (4) (Oct. 2019) 181–192.
- X. Hu, et al., Visualizing carrier transport in metal halide perovskite nanoplates via electric field modulated photoluminescence imaging, *Nano Lett.* 18 (5) (May 2018) 3024–3031.
- R. Meena, et al., Fluorescent carbon dots driven from ayurvedic medicinal plants for cancer cell imaging and phototherapy, *Heliyon* 5 (9) (Sep. 2019), e02483.
- X.-L. Qu, B. Yan, Stable Tb(III)-Based metal–organic framework: structure, photoluminescence, and chemical sensing of 2-Thiazolidinethione-4-carboxylic acid as a biomarker of CS2, *Inorg. Chem.* 58 (1) (Jan. 2019) 524–534.
- X. Huang, et al., Three-Dimensional laser-assisted patterning of blue-emissive metal halide perovskite nanocrystals inside a glass with switchable photoluminescence, *ACS Nano* 14 (3) (Mar. 2020) 3150–3158.
- X. Xiang, H. Ouyang, J. Li, Z. Fu, Humidity-sensitive CsPbBr₃ perovskite based photoluminescent sensor for detecting Water content in herbal medicines, *Sensor. Actuator. B Chem.* 346 (Nov. 2021) 130547.
- Z. Chen, S. Zhang, X. Qi, S. Liu, Q. Zhang, Y. Deng, Fluorescent quinolizinium ionic liquids (salts) with unexpectedly high quantum yields up to >99, *J. Mater. Chem.* 21 (25) (Jun. 2011) 8979–8982.
- J.-Y. Zeng, X.-S. Wang, X.-Z. Zhang, Research progress in covalent organic frameworks for photoluminescent materials, *Chem. Eur. J.* 26 (70) (2020) 16568–16581.

- [11] Y. Liu, J. Cui, K. Du, H. Tian, Z. He, et al., Efficient blue light-emitting diodes based on quantum-confined bromide perovskite nanostructures, *Nat. Photonics* 13 (2019). <https://www.nature.com/articles/s41566-019-0505-4>. (Accessed 28 September 2021).
- [12] J.-C. Jin, et al., Modulation of the structure and photoluminescence of bismuth(III) chloride hybrids by altering the ionic-liquid cations, *Inorg. Chem.* 59 (18) (Sep. 2020) 13465–13472.
- [13] Z. Li, Y. Li, P. Liang, T. Zhou, L. Wang, R.-J. Xie, Dual-band luminescent lead-free antimony chloride halides with near-unity photoluminescence quantum efficiency, *Chem. Mater.* 31 (22) (Nov. 2019) 9363–9371.
- [14] J.-C. Jin, et al., X-ray scintillation and photoluminescence of isomorphic ionic bismuth halides with [Amim]⁺ or [Ammim]⁺ cations, *Inorg. Chem. Front.* (Aug. 2021).
- [15] Y. Takeoka, K. Asai, M. Rikukawa, K. Sanui, Hydrothermal synthesis and structure of zero-dimensional organic–inorganic perovskites, *Chem. Lett.* 34 (4) (Apr. 2005) 602–603.
- [16] Hydrothermal synthesis and structural characterization of the two-dimensional networks [M(H₂O)(bpy-dicarb)]•H₂O (M=Fe, Co, Ni, Zn; bpy-dicarb=2,2'-bipyridyl-4,4'-dicarboxylic acid) - ScienceDirect. <https://www.sciencedirect.com/science/article/abs/pii/S1293255801012158>. (Accessed 29 September 2021).
- [17] W. Wang, et al., Improved stability and efficiency of perovskite via a simple solid diffusion method, *Mater. Today Phys.* 18 (May 2021) 100374.
- [18] N. Kawano, et al., Scintillating organic–inorganic layered perovskite-type compounds and the gamma-ray detection capabilities, *Sci. Rep.* 7 (1) (Nov. 2017) 14754.
- [19] J.-C. Jin, N.-N. Shen, Z.-P. Wang, Y.-C. Peng, X.-Y. Huang, Photoluminescent ionic metal halides based on s2 typed ions and aprotic ionic liquid cations, *Coord. Chem. Rev.* 448 (Dec. 2021) 214185.
- [20] N.I. Selivanov, Y.A. Rozhkova, R. Kevorkyants, A.V. Emeline, D.W. Bahnemann, The effect of organic cations on the electronic, optical and luminescence properties of 1D piperidinium, pyridinium, and 3-hydroxypyridinium lead trihalides, *Dalton Trans.* 49 (14) (Apr. 2020) 4390–4403.
- [21] N. Shen, et al., Designing polymorphic Bi³⁺-containing ionic liquids for stimuli-responsive luminescent materials, *Inorg. Chem.* 58 (12) (Jun. 2019) 8079–8085.
- [22] J.-C. Jin, et al., Long lifetime phosphorescence and X-ray scintillation of chlorobismuthate hybrids incorporating ionic liquid cations, *J. Mater. Chem. C* 9 (5) (Feb. 2021) 1814–1821.
- [23] Y.-B. Tong, L.-T. Ren, H.-B. Duan, J.-L. Liu, X.-M. Ren, An amphidynamic inorganic–organic hybrid crystal of bromoplumbate with 1,5-bis(1-methylimidazolium)pentane exhibiting multi-functionality of a dielectric anomaly and temperature-dependent dual band emissions, *Dalton Trans.* 44 (40) (Oct. 2015) 17850–17858.
- [24] Z.-P. Wang, J.-Y. Wang, J.-R. Li, M.-L. Feng, G.-D. Zou, X.-Y. Huang, [Bmim]2SbCl₅: a main group metal-containing ionic liquid exhibiting tunable photoluminescence and white-light emission, *Chem. Commun.* 51 (15) (Feb. 2015) 3094–3097.
- [25] N. Shen, et al., A- and β-[bmim][BiCl₄(2,2'-bpy)]: two polymorphic bismuth-containing ionic liquids with crystallization-induced phosphorescence, *Chem. Eur. J.* 23 (62) (2017) 15795–15804.
- [26] F. Neese, Software update: the ORCA program system, version 4.0, *WIREs Comput. Mol. Sci.* 8 (1) (2018) e1327.
- [27] A.D. Becke, Density-functional exchange-energy approximation with correct asymptotic behavior, *Phys. Rev. A* 38 (1988) 3098. <https://journals.aps.org/pr/a/abstract/10.1103/PhysRevA.38.3098>. (Accessed 10 October 2021).
- [28] C. Lee, W. Yang, R.G. Parr, Development of the Colle-Salvetti correlation-energy formula into a functional of the electron density, *Phys. Rev. B* 37 (2) (Jan. 1988) 785–789.
- [29] F. Weigend, R. Ahlrichs, Balanced basis sets of split valence, triple zeta valence and quadruple zeta valence quality for H to Rn: design and assessment of accuracy, *Phys. Chem. Chem. Phys.* 7 (18) (Aug. 2005) 3297–3305.
- [30] B. de Souza, F. Neese, R. Izsák, On the theoretical prediction of fluorescence rates from first principles using the path integral approach, *J. Chem. Phys.* 148 (3) (Jan. 2018) 34104.
- [31] G.-Y. Li, D. Liu, H. Zhang, W.-W. Li, F. Wang, Y.-H. Liang, TDDFT study on the sensing mechanism of a fluorescent sensor for fluoride anion: inhibition of the ESPT process, *Spectrochim. Acta. A. Mol. Biomol. Spectrosc.* 149 (Oct. 2015) 17–22.
- [32] B. de Souza, G. Farias, F. Neese, R. Izsák, Predicting phosphorescence rates of light organic molecules using time-dependent density functional theory and the path integral approach to dynamics, *J. Chem. Theor. Comput.* 15 (3) (Mar. 2019) 1896–1904.
- [33] M. Tavakoli, H. Ahmadvand, M. Alaei, M.A. Ranjbari, Ab-initio search for efficient red thermally activated delayed fluorescence molecules for organic light emitting diodes, *Spectrochim. Acta. A. Mol. Biomol. Spectrosc.* 246 (Feb. 2021) 118952.
- [34] Chemcraft - graphical software for visualization of quantum chemistry computations. <https://www.chemcraftprog.com>.
- [35] V. Barone, M. Cossi, Quantum calculation of molecular energies and energy gradients in solution by a conductor solvent model, *J. Phys. Chem. A* 102 (11) (Mar. 1998) 1995–2001.
- [36] I. Kaljurand, T. Rodima, I. Leito, I.A. Koppel, R. Schwesinger, Self-consistent spectrophotometric basicity scale in acetonitrile covering the range between pyridine and DBU, *J. Org. Chem.* 65 (19) (Sep. 2000) 6202–6208.
- [37] L. Kong, Z. Huang, P. Chen, H. Wang, S. Zhu, J. Yang, Enhanced intersystem crossing to achieve long-lived excitons based on inhibited molecular motion and rigid structure, *Dyes Pigments* 173 (Feb. 2020) 107886.
- [38] Y. Zhang, K. Zhang, Y. Ma, L. Lin, C.-K. Wang, J. Fan, Tunable lifetimes and efficiencies of room temperature phosphorescent liquids by modulating the length and number of alkyl chains, *Phys. Chem. Chem. Phys.* 22 (35) (Sep. 2020) 19746–19757.
- [39] D. Magde, R. Wong, P.G. Seybold, Fluorescence quantum yields and their relation to lifetimes of rhodamine 6G and fluorescein in nine solvents: improved absolute standards for quantum yields, *Photochem. Photobiol.* 75 (4) (2002) 327–334.